Solid Freeform Fabrication 2022: Proceedings of the 33rd Annual International Solid Freeform Fabrication Symposium – An Additive Manufacturing Conference
Reviewed Paper

MICROSTRUCTURE AND MECHANICAL PROPERTIES OF ADDITIVELY MANUFACTURED HAYNES 230: A COMPARATIVE STUDY OF L-PBF VS. LP-DED

Muztahid Muhammad[1,2], Rukesh Gusain[1,2], Seyed R. Ghiaasiaan[1,2], Paul R. Gradl[3], Shuai Shao[1,2], Nima Shamsaei[1,2*]

[1] National Center for Additive Manufacturing Excellence (NCAME), Auburn University, Auburn, AL 36849, USA
[2] Department of Mechanical Engineering, Auburn University, Auburn, AL 36849, USA
[3] NASA Marshall Space Flight Center, Propulsion Department, Huntsville, AL 35812, USA

[*]Corresponding author: shamsaei@auburn.edu
Phone: (334) 844-4839

Abstract

This study investigates the microstructure and room temperature mechanical properties of Haynes 230 fabricated via laser powder bed fusion (L-PBF) and laser powder directed energy deposition (LP-DED). Both L-PBF and LP-DED specimens underwent similar multiple-step heat treatments (HT): stress-relieving (1066°C for 1.5 hours), followed by hot isostatic pressing (at 1163°C and 103 MPa for 3 hours), and solution annealing (1177°C for 3 hours). Microstructural analysis was conducted employing a scanning electron microscope. Uniaxial tensile tests at room temperature were conducted to evaluate the mechanical properties. The change in microstructures after HT and tensile results for both L-PBF and LP-DED specimens were comparable. Upon HTs, the micro-segregation and dendritic microstructure observed in non-heat treated conditions were almost fully dissolved, and carbide phases (M_6C/$M_{23}C_6$) formed within grain interiors and grain boundaries in both L-PBF and LP-DED specimens. Finally, the failure mechanisms under tensile load have been studied and compared by fractography.

Keywords: Additive manufacturing, Haynes 230, laser powder bed fusion, laser powder directed energy deposition, tensile properties.

Introduction

Additive manufacturing (AM) is a state-of-the-art advance manufacturing technology that can fabricate the near-net-shape part with little to no post-processing. This revolutionary manufacturing technology is getting attention due to its numerous benefits, including reducing energy consumption and reducing carbon footprint, less material waste, lowering labor cost, and, most importantly, the capability of fabricating complex geometries. Henceforth, this manufacturing technology is particularly suitable for materials with lower machinability (e.g., Ni-base superalloys [1], Ti alloys, etc.).

Haynes 230, a solid solution strengthened Ni-base superalloy, due to its excellent high-temperature strength and resistance to oxidization, is an ideal candidate for gas turbines, heat exchangers, etc. [2,3]. However, since Haynes 230 has poor machinability [1] and many of the Haynes

230 parts constitute complex geometry, AM can be a suitable option for fabricating Haynes 230 parts. Among different AM technologies, laser powder bed fusion (L-PBF) and laser powder directed energy deposition (LP-DED) are two of the most common ones. L-PBF fabricates parts layer by layer using a laser that melts the powder evenly distributed over the build plate [4]. In LP-DED technique, powders are injected by a nozzle and simultaneously melted by a laser; the molten metal is then deposited to fabricate the parts [5].

Despite offering various advantages over traditional manufacturing techniques, the qualification and certification of AM parts for critical load-bearing applications are still challenging due to their unique microstructures and the associated variability which affects their mechanical performance [6]. In addition, AM parts fabricated via different AM technologies (e.g., L-PBF vs. LP-DED) experience different thermal histories, which may result in different microstructure (i.e., grain size, morphology, etc.) that can remain even after complete heat treatment (HT) [7]. Hence, it is necessary to investigate the mechanical properties of AM parts fabricated using different AM technologies before putting them in service applications. Although microstructure and tensile properties of solid solution strengthened Ni-base superalloys such as Haynes 230 fabricated via AM method have been studied in the literature [8–12], there is a lack of knowledge how different AM processes could affect the microstructure and mechanical properties of AM Haynes 230. Therefore, this study investigated the tensile properties of Haynes 230 alloy fabricated using L-PBF and LP-DED techniques.

Experimental Procedure

Cylindrical rods of the Haynes 230 alloy were fabricated employing both L-PBF and LP-DED. L-PBF Haynes 230 bars were fabricated using an EOS M290 machine, while LP-DED Haynes 230 specimens were fabricated using a RPM Innovations (RPMI) 557 Laser Deposition System machine. The list of the process parameters and chemical compositions of powder used for the fabrication Haynes 230 specimens in this study are included in **Table 1** and **Table 2**, respectively.

After fabrication, the cylindrical bars went through multi-steps of standard HTs, including stress-relieving (SR at 1066°C for 1.5 hr followed by air cooling), hot isostatic pressing (HIP at 1163°C under 103 MPa isostatic pressure for 3 hr followed by air cooling) [13,14], and solution annealing (SA at 1177°C for 3 hr followed by argon quench) [13–15] (see **Figure 1**). Following HT, the cylindrical rods were machined to the final geometry of the tensile test specimen according to ASTM E8 standard [16] (see **Figure 2**).

Microstructural analysis of L-PBF and L-DED Haynes 230 was conducted on the transverse plane (i.e., parallel to the build direction) of small microstructural samples obtained from the gage of tensile samples. The microstructural samples were mounted in epoxy resin and polished utilizing a mechanical polisher until mirror polish following ASTM-E3 [17]. Microstructural analysis was conducted in a Zeiss 550 scanning electron microscope (SEM) equipped with electron backscattered diffraction (EBSD) and energy dispersive spectroscopy (EDS) detectors. The electron channeling contrast imaging (ECCI) was used to capture backscattered (BSE) images of the microstructures [18]. Grain size and morphology were analyzed using EBSD analysis, and the chemical composition of the alloys was investigated using EDS.

Room temperature tensile tests were conducted at a strain rate of 0.005 mm/mm/min according to the ASTM E8 standard [16]. During testing, the specimens were pulled until complete separation, and an extensometer was attached to the specimens to record the strain experienced by the specimens for accurate determination of the yield point of the alloys. At least three specimens were tested for each data point to ensure the repeatability of the results.

Table 1. Process parameters employed in this study for fabricating L-PBF and LP-DED Haynes 230.

Fabrication technique	Power, P (W)	Layer thickness, t (µm)	Scan velocity, V (mm/sec)	Hatch distance, H (µm)	Powder feed rate (g/min)
L-PBF	300	40	1500	70	-
LP-DED	1070	381	16.93	-	19.10

Table 2. Chemical compositions (Wt.%) of powders used in this study for fabrication of LB-PBF and LP-DED Haynes 230 test specimens.

Elements	L-PBF (Wt.%)	LP-DED (Wt.%)
Ni	Bal.	Bal.
C	0.09	0.10
Mn	0.45	0.56
Si	0.33	0.55
P	-	<0.01
S	0.0016	<0.001
Cr	21.75	20.72
Mo	2.50	1.94
W	14.71	14.12
Al	0.45	0.47
La	0.01	0.012
Co	1.57	<0.01
Ti	0.08	0.04
B	<0.001	<0.001
Fe	1.84	0.14
Cu	-	0.01
N	0.01	-
O	0.01	-

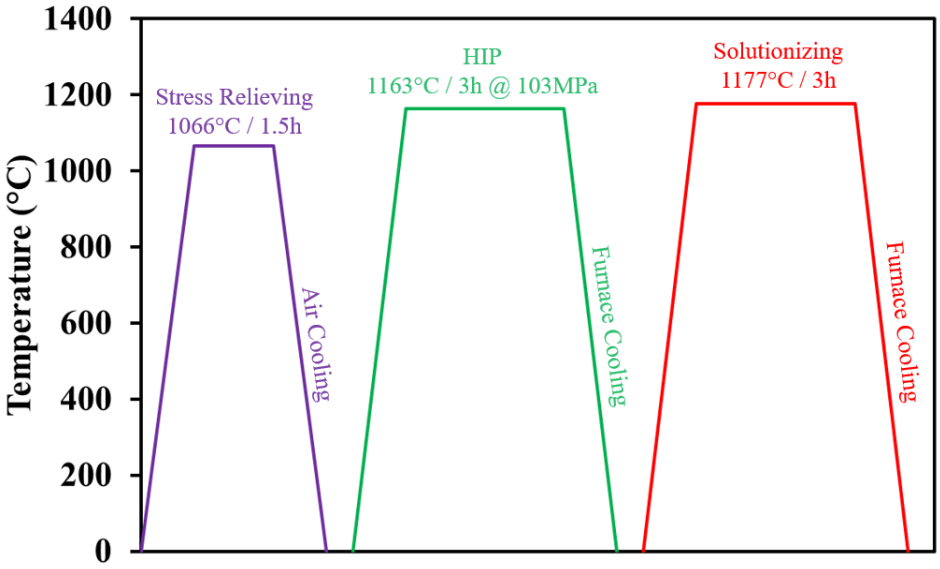

Figure 1. Schematic diagram of heat treatments conducted in this study on AM Haynes 230 specimens.

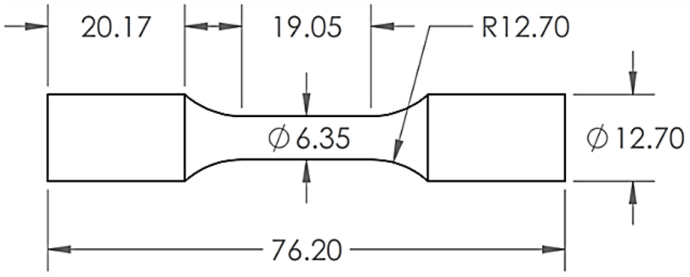

Figure 2. Geometry of L-PBF and LP-DED Haynes 230 tensile specimens. All the dimensions are in mm.

Results and Discussion

Inverse pole figure (IPF) maps of both L-PBF and LP-DED Haynes 230 specimens in both non-heat-treated (NHT) and fully heat-treated (HT) conditions obtained in the transverse plane, i.e., parallel to the build direction, are presented in **Figure 3**((a)-(d)). The average grain size of all HT conditions, along with standard deviations, are shown at the top of their respective IPF maps (see **Figure 3**((a)-(d))). The grain size measurements were obtained using EBSD analysis. Note that, the step size of EBSD scans for obtaining these IPF maps was 4.3 µm, therefore, grains smaller than 4.3 µm were not detected. As shown in **Figure 3**((a)-(d)), the grains are columnar in shape, which is typical grain morphology for AM parts in the plane parallel to the build direction. There is no apparent effect of full HT on the average grain size of both L-PBF (~ 40 µm) and LP-DED (~ 60 µm) Haynes 230 specimens. In addition, the average grain size of LP-DED specimens is slightly larger (factor of ~ 1.5) than L-PBF specimens, which can be attributed to the differences in thermal history, i.e.,

differences in their feedstock [19] and process parameters of these techniques [20]. In addition, LP-DED Haynes 230 consisted of relatively large grains along with the regular size grains (standard deviation ~ 85 µm) compared to the L-PBF ones (standard deviation ~ 30 µm). This variation of grain size between L-PBF and LP-DED Haynes 230 might affect their mechanical performance (e.g., tensile strength).

BSE micrographs of NHT and HT L-PBF and LP-DED Haynes 230 specimens obtained through ECCI technique are shown in **Figure 3**((g)-(h)). In NHT condition, both L-PBF and LP-DED specimens consisted of dendritic microstructure (the interdendritic regions are indicated by yellow arrows in **Figure 3**((g)-(h))). In addition, severe micro-segregation in the γ matrix was also observed for both alloys in NHT condition. Upon full HT, dendritic structures were almost dissolved. In addition, the metal carbides formed along the grain boundaries (GBs). Haynes 230 superalloy is known to form Mo-rich (M_6C) and Cr-rich ($M_{23}C_6$) carbides [11,21] and EDS analysis conducted on the HT L-PBF and LP-DED Haynes 230 specimens indicates their formation (see **Figure 4**). These carbides can strengthen the GBs specially at elevated temperatures by obstructing GB sliding [22].

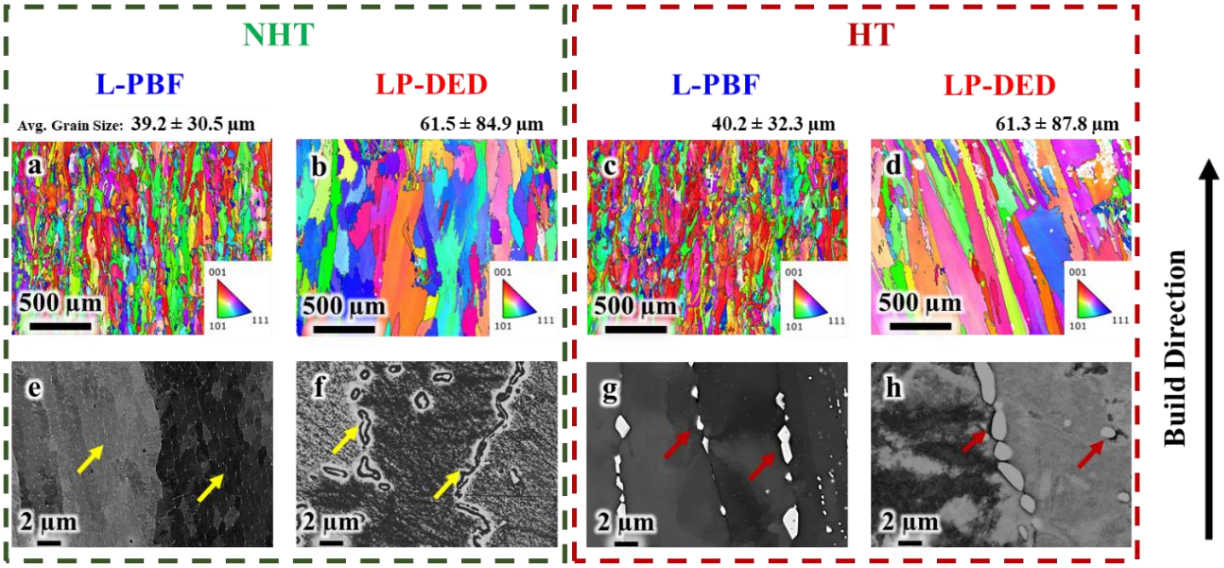

Figure 3. IPF maps obtained from EBSD analysis for L-PBF and LP-DED specimens in (a)-(b) NHT and (c)-(d) fully HT conditions; and BSE micrographs of L-PBF and LP-DED specimens in (e)-(f) NHT and (g)-(h) fully HT conditions. Yellow arrows indicate interdendritic regions and red arrows indicate metal carbides at GBs.

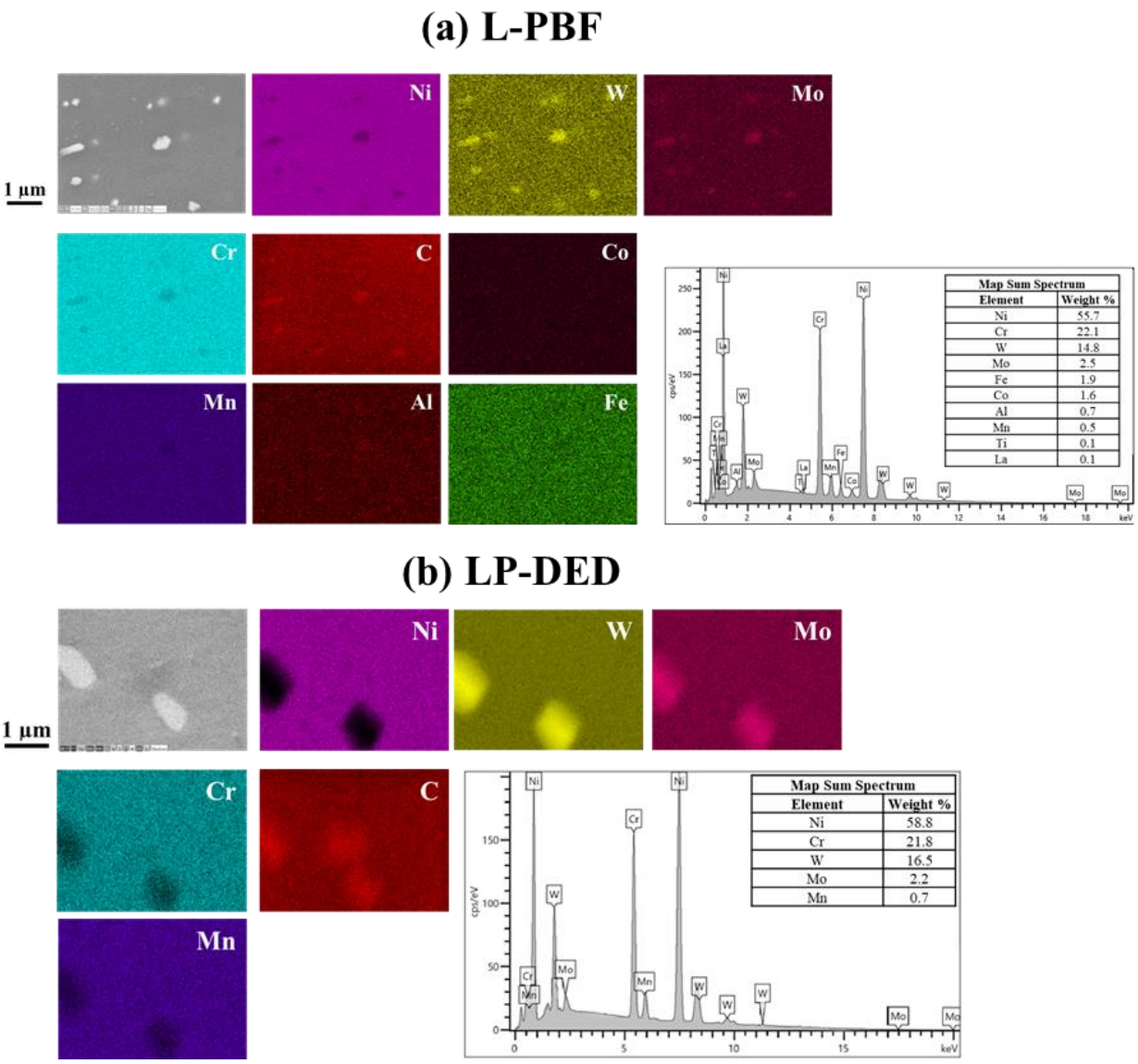

Figure 4. EDS analysis of fully HT (a) L-PBF and (b) LP-DED Haynes 230 specimens.

Engineering stress-engineering strain curves of fully HT L-PBF and LP-DED Haynes 230 are shown in **Figure 5**. The comparative column charts for the tensile properties (yield strength, S_y, ultimate tensile strength, S_u, and percent elongation to failure, %EL) of fully HT L-PBF, LP-DED, and wrought (collected from [3]) Haynes 230 are also presented in **Figure 6**. In addition, fracture surfaces of both L-PBF and LP-DED Haynes 230 tensile specimens are also shown in **Figure 7**. As shown in **Figure 5** and **Figure 6**, L-PBF Haynes 230 specimens exhibit higher tensile strengths (~26% higher S_y and ~7% higher S_u) as compared to the LP-DED ones. The higher tensile strength of L-PBF specimens can be attributed to their finer grain structure with smaller average grain size (see **Figure 3**) compared to LP-DED ones. According to the Hall-Petch relationship [23], the yield strength of metal alloys is inversely proportional to the grain size, i.e., the smaller the grain size, the higher the yield strength. In addition, LP-DED specimens showed slightly higher ductility (~11% higher %EL) compared to L-PBF one, and both L-PBF and LP-DED Haynes 230 showed significant ductility (40%

and 45% %EL, respectively). As shown in **Figure 7**, fine dimples (indicated by red arrows) and cup-and-cone features on the fracture surfaces of both L-PBF and LP-DED Haynes 230 are the indicators of ductile fracture, which is consistent with other solid solution strengthening Ni-base superalloys; Ghiaasiaan et al. [10] and Muhammad et al. [12] reported more than 40% EL for L-PBF Hastelloy-X and LP-DED Haynes 230 in solution annealed condition. Comparing the tensile properties of AM Haynes 230 with the wrought one collected from [3] in (see **Figure 6**), it is observed that the tensile strength (i.e., S_y and S_u) of L-PBF and wrought Haynes 230 are comparable. Furthermore, the ductility (i.e., %EL) of LP-DED and wrought Haynes 230 are almost similar.

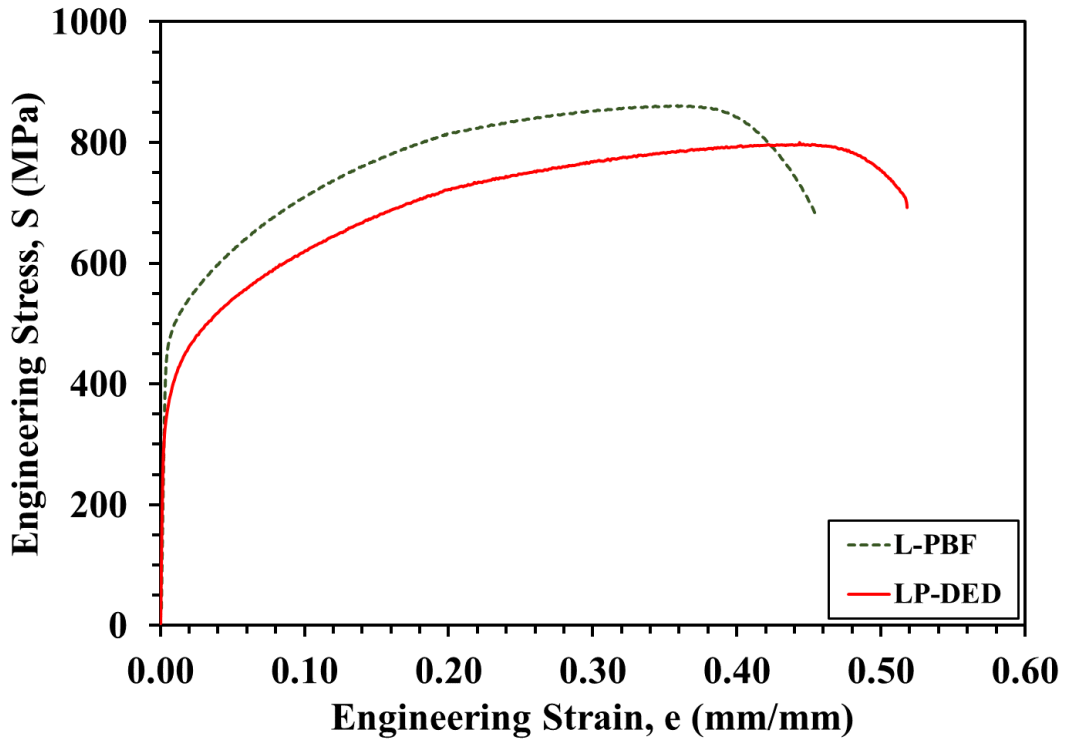

Figure 5. Engineering stress-engineering strain for fully HT L-PBF and LP-DED Haynes 230 specimens.

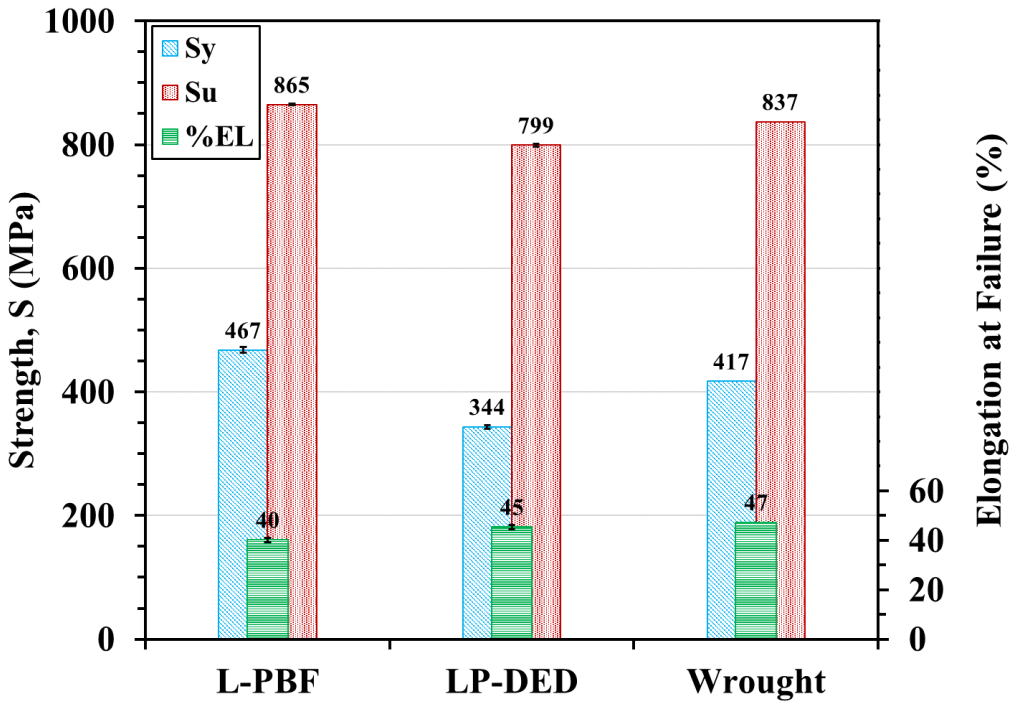

Figure 6. Column charts showing tensile properties (yield strength, S_y, ultimate tensile strength, S_u, and percent elongation at failure, %EL) of fully HT L-PBF, LP-DED, and wrought [3] Haynes 230 specimens.

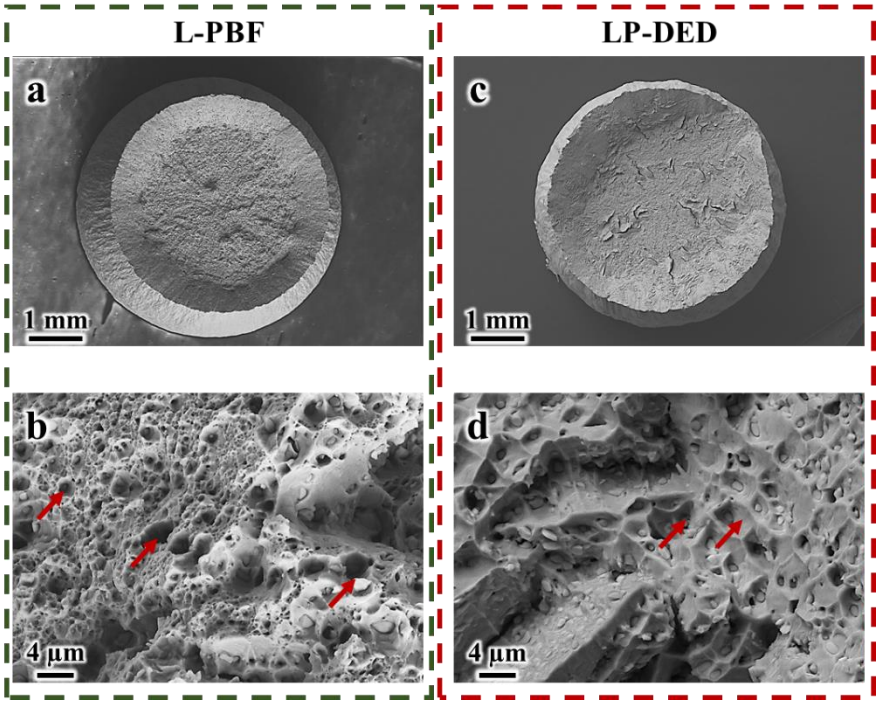

Figure 7. Tensile fracture surfaces of Haynes 230: (a)-(b) L-PBF and (c)-(d) LP-DED. Red arrows indicate the dimples.

Conclusions

This study compared the microstructure and tensile properties of L-PBF and LP-DED Haynes 230 upon full HT (i.e., SR, HIP, and SA). Tensile properties were correlated with microstructure and fracture surfaces. The findings of this study can be summarized as:

- In NHT conditions, both L-PBF and LP-DED specimens consist of dendritic microstructure and severe micro-segregation, all of which upon full HT were partially dissolved into γ matrix.
- L-PBF Haynes 230 consists of finer grain structure as compared to the LP-DED one. Moreover, full HTs did not affect the grain morphology of both L-PBF and LP-DED Haynes 230.
- L-PBF Haynes 230 exhibited higher tensile strength as compared to LP-DED ones, which can be attributed to the finer grain structure in L-PBF specimens.
- Upon full HT, both L-PBF and LP-DED Haynes 230 specimens showed significantly high ductility (more than ~40% percent elongation to failure), which is comparable to the ductility of wrought Haynes 230 reported in the literature.

Acknowledgment

This research is partially supported by the National Aeronautics and Space Administration NASA under Cooperative Agreement No. 80MSFC19C0010. This paper describes objective technical results and analysis. Any subjective views or opinions that might be expressed in the paper do not necessarily represent the views of the National Aeronautics and Space Administration (NASA) or the United States Government.

References

[1] I. Choudhury, M. El-Baradie, Machinability of nickel-base super alloys: a general review, J. Mater. Process. Technol. 77 (1998) 278–284.
[2] C.J. Boehlert, S.C. Longanbach, A comparison of the microstructure and creep behavior of cold rolled HAYNES® 230 alloy™ and HAYNES® 282 alloy™, Mater. Sci. Eng. A. 528 (2011) 4888–4898.
[3] HAYNES ® 230 ® alloy, 2021.
[4] S. Bremen, W. Meiners, A. Diatlov, Selective Laser Melting, Laser Tech. J. 9 (2012) 33–38.
[5] M. Molitch-Hou, Overview of additive manufacturing process, Addit. Manuf. (2018) 1–38.
[6] A. Yadollahi, N. Shamsaei, Additive manufacturing of fatigue resistant materials: Challenges and opportunities, Int. J. Fatigue. 98 (2017) 14–31.
[7] M. Muhammad, R. Ghiaasiaan, P.R. Gradl, A. Schobel, D. Godfrey, S. Shao, N. Shamsaei, Additively manufactured Hastelloy-X: effect of post-process heat treatment on microstructure and mechanical properties, Proc. 32nd Solid Free. Fabr. Symp. (2021) 923-934.
[8] T. Bauer, K. Dawson, A. Spierings, K. Wegener, Microstructure and mechanical characterisation of SLM processed Haynes® 230®.
[9] R. Ghiaasiaan, A. Poudel, N. Ahmad, M. Muhammad, P.R. Gradl, S. Shao, N. Shamsaei, Room Temperature Mechanical Properties of Additively Manufactured Ni-base Superalloys:

A Comparative Study, Procedia Struct. Integr. 38 (2022) 109–115.
[10] R. Ghiaasiaan, M. Muhammad, P.R. Gradl, S. Shao, N. Shamsaei, Superior tensile properties of Hastelloy X enabled by additive manufacturing, Mater. Res. Lett. 9 (2021) 308–314.
[11] M. Haack, M. Kuczyk, A. Seidel, E. López, F. Brueckner, C. Leyens, Comprehensive study on the formation of grain boundary serrations in additively manufactured Haynes 230 alloy, Mater. Charact. 160 (2020) 110092.
[12] M. Muhammad, R. Ghiaasiaan, P.R. Gradl, S. Shao, N. Shamsaei, Additively manufactured Haynes 230 by laser powder directed energy deposition (LP-DED): effect of heat treatment on microstructure and tensile properties, Proc. 32nd Solid Free. Fabr. Symp. (2021) 935-947.
[13] G. Marchese, E. Bassini, A. Aversa, M. Lombardi, D. Ugues, P. Fino, S. Biamino, Microstructural Evolution of Post-Processed Hastelloy X Alloy Fabricated by Laser Powder Bed Fusion, Materials (Basel). 12 (2019) 486.
[14] D.A.A. Sadek Tadros, D.G.W. Ritter, C.D. Drews, D. Ryan, Additive Manufacturing of Fuel Injectors, Pittsburgh, PA, and Morgantown, WV (United States), 2017.
[15] HASTELLOY ® X ALLOY A nickel-base alloy with an exceptional combination of oxidation resistance, fabricability and high-temperature strength. H-3009A, 1997.
[16] ASTM International, ASTM E8/E8M-16: Standard Test Methods for Tension Testing of Metallic Materials, (2016).
[17] A.E.− 11 Interanational, Standard Guide for Preparation of Metallographic Specimens Standard Guide for Preparation of Metallographic Specimens 1, ASTM Int. 03.01 (2012) 1–12.
[18] S. Zaefferer, N.-N. Elhami, Theory and application of electron channelling contrast imaging under controlled diffraction conditions, Acta Mater. 75 (2014) 20–50.
[19] M. Muhammad, P.D. Nezhadfar, S. Thompson, A. Saharan, N. Phan, N. Shamsaei, A comparative investigation on the microstructure and mechanical properties of additively manufactured aluminum alloys, Int. J. Fatigue. 146 (2021) 106165.
[20] P.D. Nezhadfar, P.R. Gradl, S. Shao, N. Shamsaei, Microstructure and Deformation Behavior of Additively Manufactured 17–4 Stainless Steel: Laser Powder Bed Fusion vs. Laser Powder Directed Energy Deposition, JOM. 74 (2022) 1136–1148.
[21] K. Hrutkay, D. Kaoumi, Tensile deformation behavior of a nickel based superalloy at different temperatures, Mater. Sci. Eng. A. 599 (2014) 196–203.
[22] On the theory of the effect of precipitate particles on grain growth in metals, Proc. R. Soc. London. Ser. A. Math. Phys. Sci. 294 (1966) 298–309.
[23] G.E. Dieter, Mechanical Metallurgy, 3rd ed., McGraw-Hill, Boston, MA, MA, 1986.